Monthly Notices of the ROYAL ASTRONOMICAL SOCIETY

Mon. Not. R. Astron. Soc. **422,** 1219–1230 (2012) doi:10.1111/j.1365-2966.2012.20700.x

Serendipitous *Kepler* observations of a background dwarf nova of SU UMa type

Thomas Barclay,[1,2★] Martin Still,[1,2] Jon M. Jenkins,[3] Steve B. Howell[1] and Rachael M. Roettenbacher[4]

[1]*NASA Ames Research Center, M/S 244-40, Moffett Field, CA 94035, USA*
[2]*Bay Area Environmental Research Institute, Inc., 560 Third Street West, Sonoma, CA 95476, USA*
[3]*SETI Institute/NASA Ames Research Center, Moffett Field, CA 94035, USA*
[4]*Deptartment of Astronomy, University of Michigan, 830 Dennison Building, 500 Church Street, Ann Arbor, MI 48109, USA*

Accepted 2012 February 3. Received 2012 February 3; in original form 2011 December 1

ABSTRACT

We have discovered a dwarf nova (DN) of type SU UMa in *Kepler* data which is 7.0 arcsec from the G-type exoplanet survey target KIC 4378554. The DN appears as a background source in the pixel aperture of the foreground G star. We extracted only the pixels where the DN is present and observed the source to undergo five outbursts – one a superoutburst – over a time span of 22 months. The superoutburst was triggered by a normal outburst, a feature that has been seen in all DNe superoutbursts observed by *Kepler*. Superhumps during the superoutburst had a period of 1.842 ± 0.004 h, and we see a transition from disc-dominated superhump signal to a mix of disc and accretion stream impact. Predictions of the number of DNe present in *Kepler* data based on previously published space densities vary from 0.3 to 258. An investigation of the background pixel targets would lead to firmer constraints on the space density of DNe.

Key words: accretion, accretion discs – methods: data analysis – stars: dwarf novae – novae, cataclysmic variables.

1 INTRODUCTION

Cataclysmic variables (CVs) are binary star systems consisting of a white dwarf primary and a less massive main-sequence or post-main-sequence secondary. The two stars orbit a common centre of mass with typical periods between 50 min and 5.7 d (Sekiguchi 1992; Downes et al. 2001; Ritter & Kolb 2003; Thorstensen, Lépine & Shara 2006). The small physical size of the binary system causes the secondary to be distorted by the gravitational field of the white dwarf and leads to the filling of its Roche lobe. Mass is transferred through the L1 inner Lagrangian point and forms a stream of material falling into the potential well of the white dwarf. In the case where the white dwarf is non-magnetic, the infalling material forms an *accretion disc* (Shakura & Sunyaev 1973). Viscous shearing layers amplify a weak magnetic field within the disc, and lead to turbulent angular momentum transport radially outwards (Balbus & Hawley 1998). Mass can then move inwards and be accreted on to the surface of the white dwarf (Hellier 2001). At optical wavelengths, the disc is usually much more luminous than the white dwarf, its companion and the impact of the accretion stream on to the disc.

The DN subclass of CVs undergo quasi-periodic outbursts (see Warner 2003, for a review). During an outburst, the optical brightness of the system can increase by a factor of 10 or more (e.g. Ramsay et al. 2009), which interrupts the faint *quiescent* state in which the DNe typically spend most of their time.

If the mass transfer rate from the secondary to the accretion disc is greater than the rate of disc accretion on to the white dwarf, $\dot{M}(2) > \dot{M}(d)$, then the disc radius will increase over time. This can only happen if the dimensionless disc viscosity parameter α is low (where low is usually taken in models to be $\lesssim 0.03$; e.g. Smak 1984; Cannizzo 1993). The disc instability model predicts that eventually the surface density in the disc will exceed a critical value $\Sigma_{\rm max}$, which initiates a phase transition in the disc material (Hōshi 1979; Lasota 2001). At this point, the α parameter increases (by a factor of $\sim$10; Smak 1984; Cannizzo 1993) and $\dot{M}(2) < \dot{M}(d)$ for a time until the surface density at the outer edge of the disc decreases below some critical surface density $\Sigma_{\rm min}$, and α returns to the original lower value. This model is known as the limit cycle accretion disc instability (Lasota 2001).

A subset of DNe known as SU UMa stars occasionally undergo a superoutburst (SO) in addition to undergoing normal outbursts (NO). SOs are typically a factor of 2 brighter and 5–10 times longer than a NO (Warner 2003). Superhumps, photometric variability on a period a few per cent longer than the orbital period of the system,

★E-mail: thomas.barclay@nasa.gov

© 2012 The Authors
Monthly Notices of the Royal Astronomical Society © 2012 RAS

Table 1. Log of *Kepler* observations of KIC 4378554 up to BJD 245 5635. The start and end BJD refer to the mid-time of the first and last cadences on which there are no flags questioning the quality of the data. We find the data quality flags in the light curve and target pixel files under the column SAP_QUALITY – non-zero indicates a potentially compromised cadence (the specific meaning of each flag is given in the Kepler Archive Manual; Fraquelli & Thompson 2011). Likewise, the number of cadences column in this table excludes cadences which contain potentially compromised data.

Quarter	Start BJD (−245 4900)	End BJD (− 245 4900)	# cadences	Module	Output	Channel
1	64.5115	97.9832	1611	15	3	51
2	102.7648	191.4672	4048	3	3	7
3	193.2449	282.4947	4099	11	3	35
4	285.3758	375.2017	4092	23	3	79
5	376.5095	471.1621	4460	15	3	51
7	563.1953	652.5473	4190	11	3	35
8	668.3827	735.3435	3098	23	3	79

are observed during the SO. During a NO, the disc expands in radius (Osaki 1989). After a number of these outbursts, the disc can become large enough to grow beyond the inner Lindblad resonance, close to the 3:1 corotation resonance with the binary orbital period (Whitehurst 1988). Once there is enough mass at this resonance radius, the superhump oscillation can be driven by tides.

We identified a background source in *Kepler* spacecraft archival data whose light curve resembled that of a DN. In Section 2 we describe the observations made by the *Kepler* spacecraft of this source, our re-extraction of the light curve from pixel level data using a more appropriate pixel aperture and our removal of systematic photometric effects from the flux time series. In Section 3 we discuss observed outbursts, and in Section 4 we discuss the implications of these observations on the nature of outbursts from DN.

2 OBSERVATIONS

Kepler has been almost continuously observing over 1.6×10^5 stars at a cadence of 30 min (Borucki et al. 2010; Koch et al. 2010) at millimagnitude to micromagnitude precision (Gilliland et al. 2011) since the spacecraft's launch on 2009 March 06. While the primary aim of the *Kepler* mission is the discovery of exoplanets, the long baseline of continual, high-precision observations has also provided an unrivalled data set to the stellar astrophysics community.

The available bandwidth does not allow all starlight falling on to the *Kepler* detectors to be downloaded at a cadence of 30 min. Instead, the pixels to be collected must be preselected and account for only 5.75 per cent of the total detector area available (Koch et al. 2010).

The continuity of observations are broken every month by the satellite pointing towards Earth for data to be downloaded. Once every three months, the satellite rolls 90° to keep the sunshade pointed in the appropriate direction but has the effect of changing the CCD that a star falls upon every quarter. Because of the change in physical position of the instrument and because a new data set is downloaded, the data from *Kepler* are divided into quarters starting with Quarter 0 (Q0), containing commissioning observations, and full science operations beginning in Q1.

Each observed star is extracted by selecting a pixel mask which can change in size and shape every quarter because the position of the star in pixel space is different. For this reason, the contamination from background stars is different every quarter – this contamination can be significant because part of the *Kepler* field covers the Galactic plane (where the stellar density is high) and the pixels are relatively large (3.98×3.98 arcsec^2).

The observations described in this paper are of one particular target aperture – that around KIC 4378554. This star was chosen to be a target in the *Kepler* exoplanetary programme. *Kepler* observed KIC 4378554 during Q1–Q8 excluding Q6 (see Table 1 for a log of the observations). No planet has been found transiting this system as yet. The *Kepler* Input Catalogue lists KIC 4378554 as a $Kp = 14.9$ star[1] with colour $(g' - r') = 0.57$, an effective temperature of 5617 K and a surface gravity of $\log g = 4.615$ in cgs units; these values are consistent with the source being a main-sequence G-type star (Brown et al. 2011). The star is only visible during three of the four seasons of observations because it lies on Module 3 for one quarter. Module 3 failed during Q4.

2.1 Optimal aperture observations

Two light-curve products are provided by the *Kepler* project: light curves extracted using Simple Aperture Photometry (SAP) and light curves which have undergone the additional step of Pre-Search Data Conditioning (PDC; Twicken et al. 2010). The latter of these is produced for use in exoplanet searches but is known to cause problems if used for stellar astrophysics work. These problems include the attenuation of astrophysical signal and the injection of spurious signals; because of this, we use the SAP data. A light curve showing Q5 data can be seen in Fig. 1. These data have not had systematic artefacts removed, and there are several noticeable features due to systematics such as the increase in flux level over the final 50 d of the quarter and the thermal settling after Earth-points at Barycentric Julian Date (BJD) 245 5307 and 245 5337. However, there is one obvious feature that appears to be astrophysical in nature – a 2 per cent increase in brightness with a peak at BJD 245 5342.8 lasting 2.5 d. In addition to the brightening shown here, we identified four similar events – two in Q3, one in Q4 and one in Q7. Events like these are not typically seen in G-type stars and therefore warranted further investigation.

2.2 Custom light-curve extraction from target pixel files

In order to determine whether the brightness increases are due to KIC 4378554 or a background star in the optimal aperture of KIC

[1] *Kp* refers to approximate *Kepler* instrumental magnitudes. For more details on this passband, see Brown et al. (2011).

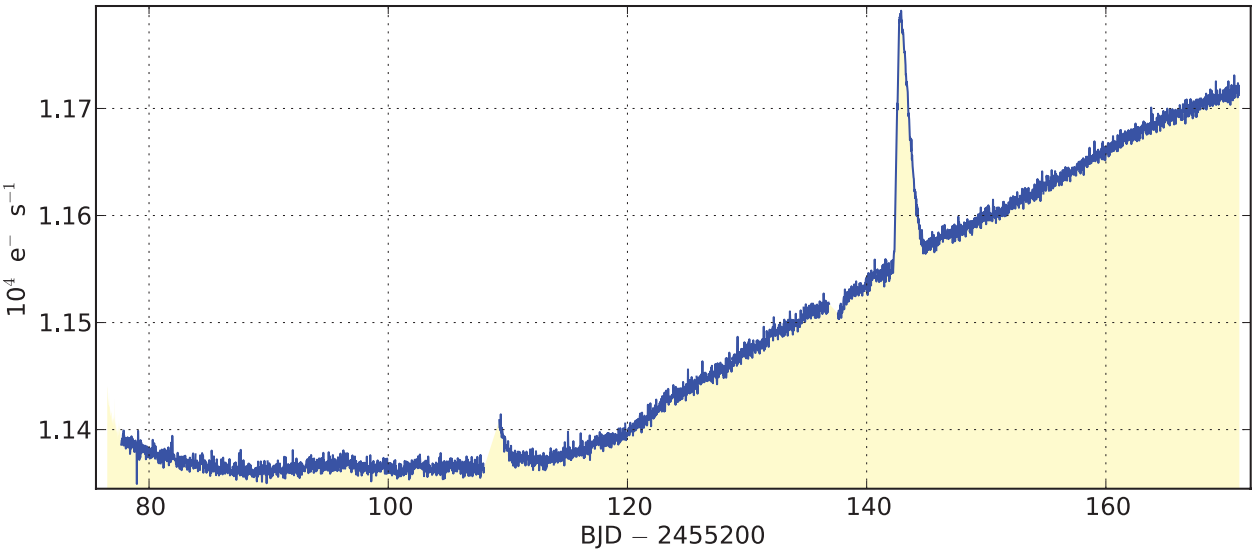

Figure 1. The Q5 SAP light curve made using the optimal aperture calculated for KIC 4378554. The light curve contains systematics, such as differential velocity aberration, which causes the change in the general flux level over the last 50 d of the quarter, and a data gap from Earth-point followed by a thermal settling at BJD 245 5307 and then again at BJD 245 5337. In addition, there is a sudden, temporary 2 per cent increase in the flux level, reaching a peak at BJD 245 5342.8.

4378554, we examined the archived target pixel files.[2] These files contain a series of images – one for each time stamp – showing the individual pixels downloaded from the *Kepler* spacecraft. These images were calibrated by the *Kepler* pipeline (as described by Quintana et al. 2010). Shown in Fig. 2 is the Q5 time series for each calibrated pixel in the aperture of KIC 4378554. The pixels shown in grey were used to create the light curve in Fig. 1. From Fig. 2 we can see that the brightness increase at BJD 245 5342.8 is not caused by KIC 4378554 but by a source which appears to have its centre on or close to pixel (1043 857) approximately 1.5 pixels south-west of the target star. For convenience, we will refer to this source as NIK 1 (standing for not in KIC).

We extracted a new light curve by summing only those pixels which NIK 1 contributes flux using the KEPMASK and KEPEXTRACT tools from the PYKE *Kepler* community software.[3] In quarters where we see a sudden brightening event, this is relatively straightforward. This is the case in Q3, Q4, Q5 and Q7. For Q1 we use the Q5 aperture, and for Q8 we used the Q4 aperture because NIK 1 will be at the same position on the CCD four quarters apart. For Q2 we estimate the position of NIK 1 from the full-frame image taken at the end of Q3, when a brightening event occurred and NIK 1 is visible.[4] We overlaid the full-frame image containing NIK 1 on the pixel level data and selected the appropriate pixels. The number of pixels we use for all quarters is listed in Table 2.

2.3 Removing systematic trends using cotrending basis vectors

The light curves we extracted from target pixel files still contain systematic features. This is because the extracted aperture does not contain all the flux and also contains contaminating flux from the target star, KIC 4378554. The amount of flux in the aperture, both from NIK 1 and from other contaminating sources, changes continually over time due to differential velocity aberration and suddenly due to changes in the focus after Earth-points (Christiansen et al. 2011a).

The instrumental systematics which affect a single light curve are unique. However, we see strong correlations between stars which are on the same CCD channel. We can take those stars which are most highly correlated, which we call the reference ensemble, and identify the correlated features. These correlations can be represented as linear combinations of orthogonal vectors, which can be fitted and subtracted from each individual light curve to remove instrumental features. The *Kepler* team have created a product containing these vectors, known as cotrending basis vectors (CBVs), and have made them available to the public[5] [a description of how they were created is given in Christiansen et al. (2011b) and Barclay et al. (2011)].

The available files consist of the 16 vectors, of length the same as the light curve, which provide the greatest contribution to the variance of the reference ensemble. There is one set of 16 vectors per quarter for every CCD readout. It is crucial that an appropriate number of vectors are chosen to fit to the light-curve data; using too few will leave instrumental signal in the light curve, while using too many will cause overfitting and remove astrophysical signal.

We used the KEPCOTREND tool from PYKE to perform a linear least-squares fit of the CBVs to the light curve we extracted using KEPEXTRACT and masked the regions where the brightening events occur out of the fit because these regions are dominated by astrophysical signal, not systematics. We selected the number of CBVs to fit by experimenting with the fit: we assumed that there was no intrinsic long-period variability outside of the brightening and attempted to remove any long-term trends. Starting with two CBVs, we iteratively increased the number of CBVs until the regions outside of

[2] *Kepler* target pixel and light curve files are distributed at http://archive.stsci.edu/kepler.

[3] PYKE is available from http://keplergo.arc.nasa.gov/ContributedSoftware.shtml.

[4] *Kepler* full-frame images are collected once a month and are available from http://archive.stsci.edu/kepler/ffi/.

[5] CBVs are available from http://archive.stsci.edu/kepler/cbv.html.

© 2012 The Authors, MNRAS **422,** 1219–1230
Monthly Notices of the Royal Astronomical Society © 2012 RAS

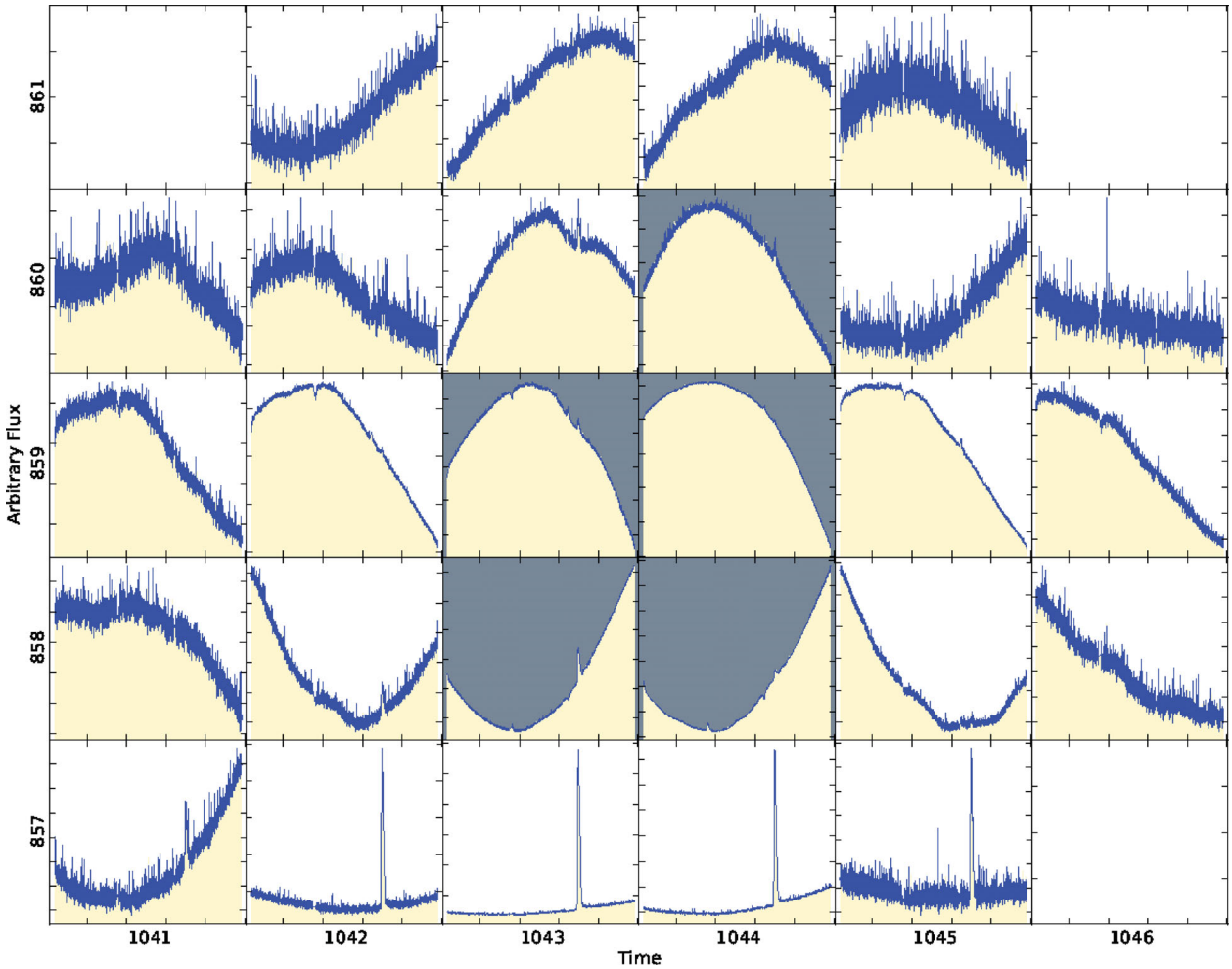

Figure 2. Plotted is the flux time series within each pixel collected for KIC 4378554 during Q5, where a quarter is the number of days between each spacecraft roll. The quarter length is typically 91 d but can vary because of, for example, spacecraft anomalies. The numbering around the plot provides the pixel column and row on the CCD channel. The blank boxes contain pixels that were not within the pixel mask. The five boxes with the grey background are those within the optimal aperture of KIC 4378554 and were used to make the plot shown in Fig. 1 and the archived light curve at the Multimission Archive at STScI (MAST). The brightening event is not coming from the source within the optimal aperture but from another source on the bottom edge of the pixel mask. The flux range is scaled separately for each pixel, the amount of scatter in each pixel is indicative of the signal-to-noise ratio of the data in that pixel. Differential velocity aberration causes KIC 4378554 to move towards the lower-left corner over the length of the quarter. The thermal settlings cause KIC 4378554 to move from left to right.

Table 2. Pixels used to extract the light curve of NIK 1 in the optimal and custom apertures, the time spans masked out of the CBV fit and the number of basis vectors used in these fits.

Quarter	Pixels in optimal ap.	Pixels in custom ap.	Time range masked in CBV fit (BJD −245 4900)	# of CBVs in fit
1	6	2		3
2	5	1		3
3	6	5	272.714 65–282.501 47	5
4	4	2	285.359 80–293.986 26	5
5	5	2	441.891 37–448.345 35	6
7	6	5	621.906 76–629.788 12	6
8	4	2		3

the brightening events was approximately constant. The number of CBVs used and the regions masked from the fit are listed in Table 2.

The CBVs only correct for the amplitude of systematic effects and not for constant offsets caused by differences between the contamination from nearby sources and changes in the fraction of flux of NIK 1 in the pixel aperture in different quarters. After removing the instrumental systematics, there are still differences between the median flux levels between quarters. To mitigate the effects of this, we normalize the light curve. A representation of the true flux level was obtained by first normalizing independently for each

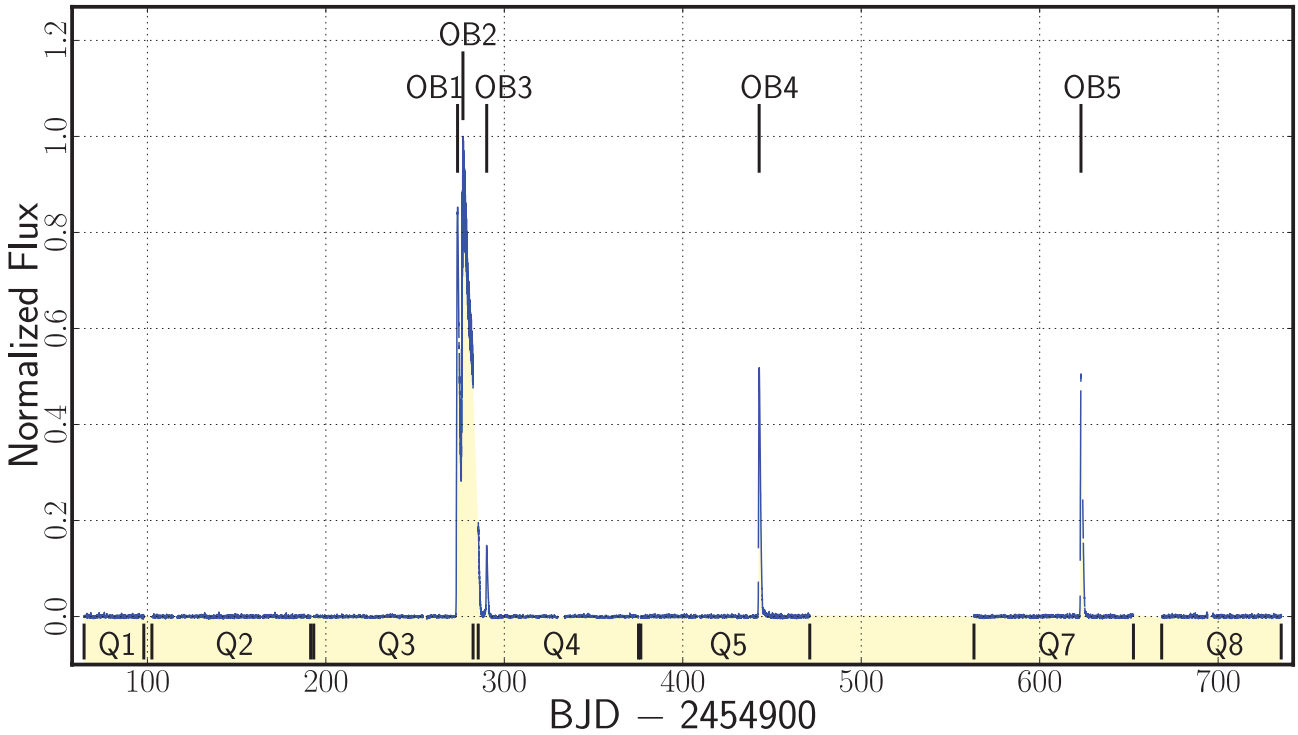

Figure 3. The fully processed light curve of NIK 1 showing seven quarters of data. The flux time series has been extracted from the target pixel files, corrected by fitting and subtracting the CBV and normalized with weights. The normalization was done by first dividing each quarter of data by its median and then dividing this value by the median absolute deviation of the corrected time series. We then divided the whole data set by the median flux of that data. The five outbursts we observed are marked with OB1–5, and beneath the time series is shown the quarter over which the data were taken.

quarter:

$$F_{\mathrm{norm},i} = \frac{F_i - \mathrm{med}\,(F)}{\mathrm{MAD}\,(F)}, \tag{1}$$

where F_{norm} is the vector of normalized fluxes, F is the vector of non-normalized fluxes, F_i is the ith element of vector F, med(F) is the median of F and MAD(F) is the median absolute deviation from the median (MAD) of F. MAD is defined as

$$\mathrm{MAD}\,(F) = \mathrm{med}\,(|F_i - \mathrm{med}\,(F)\,|)\,. \tag{2}$$

We show the full custom extracted and cotrended time series containing seven quarters of data in Fig. 3. The light curve is that of a SU UMa type DN [cf. the adapted light curve of VW Hyi from Bateson (1977) shown in Warner (2003)]. We observe five outbursts (labelled OB1–5 in Fig. 3): four NOs and one SO. One of the NOs (OB1) immediately precedes the SO (OB2), while another NO (OB3) is of much lower intensity than the other NOs and occurs a mere 4 d after the end of OB2. Our method of normalization is relatively crude; if, for example, there are significantly different levels of contamination or the noise level was dramatically different between the quarters, we would be incorrectly estimating the relative outburst amplitudes. We gain confidence that the normalization is appropriate for the following reasons: the outbursts in Q5 and Q7 are of comparable intensities, and there is a relatively smooth transition from the tail of the SO seen in Q3 and into Q4. It is possible that we are severely underestimating the amplitude in Q4 and OB3 is actually of comparable intensity to OB1, OB4 and OB5, but this would require a sharp break in the decline of the SO in the data gap between Q3 and Q4.

2.4 Archival observations

We were unable to locate NIK 1 in quiescence in *Kepler* full-frame images which have a limiting magnitude of $Kp \sim 20$, and so we looked to archival data to find NIK 1 in a quiescent state. Palomar Sky Survey I and II (POSS-I and II) observations appear in the USNO-B1.0 catalogue (Monet et al. 2003). USNO-B1.0 lists a source offset (in the direction of KIC 4378554) from NIK 1 × 2.7 arcsec. The POSS-I blue magnitude of this source is given as 19.15 and the source is catalogued as USNO-B1 1294-0347652. They again find this source in the POSS-II blue image and derive a blue magnitude of 15.13.

POSS-I and II images are available for this region as part of the Digitized Sky Survey (DSS). We examined the POSS-II images of this region and found a source we estimate to be at $B \simeq 17.3$ based on the brightness of nearby stars in the blue image, much brighter than the detection limit of the full-frame images where we do not detect NIK 1. We deduce that this source is NIK 1 in a state of outburst. Fig. 4 shows a comparison between the POSS-II red and blue images which were taken at different epochs. No source is detected at the position of NIK 1 in the red image.

Despite the USNO-B1.0 listing a source at the same position in POSS-I blue data, we were unable to locate any source. However, the fact that the source is listed with two quite different brightness measurements leaves us in little doubt that USNO-B1 1294-0347652 and NIK 1 are one and the same.

3 OUTBURSTS

The *Kepler* data contain observations of five outbursts: four NOs and one SO. The dates the outbursts reach the maximum and their rise and fall durations are given in Table 3.

© 2012 The Authors, MNRAS **422,** 1219–1230
Monthly Notices of the Royal Astronomical Society © 2012 RAS

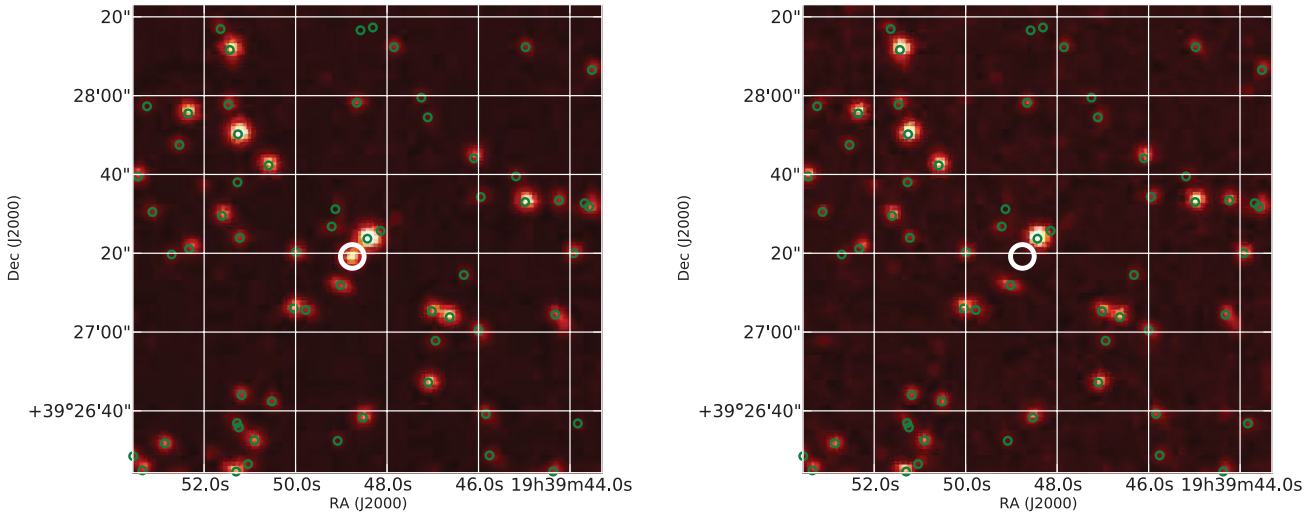

Figure 4. The DSS2 blue image taken on JD 244 7351.8 is shown in the left-hand panel and the DSS2 red image taken on JD 244 8508.7 in the right-hand panel. Circled in white on the right-hand panel is a source in the same position as we identified NIK 1 in the *Kepler* images. A white circle is drawn in the same position in the left-hand panel, but no source is detected. The green markers are the positions of sources which are in the *Kepler* Input Catalogue; no source exists in the catalogue at the position where we have detected the outbursting star.

Table 3. Outburst occurrences.

Outburst	Quarter	Type of outburst	BJD of F_{max}	T_{rise}	T_{fall}
1	3	Normal	245 5173.85	1.08	1.96[a]
2	3	Super	245 5176.86	1.05[b]	10.42
3	4	Normal	245 5190.10	1.25	1.86
4	5	Normal	245 5342.84	0.86	2.57
5	7	Normal	245 5523.17	0.81	2.39

[a]The fall time is truncated by the onset of the SO.
[b]The rise time is truncated by the tail of the first NO.

3.1 Normal outbursts

The four NOs are shown in detail in Figs 5 and 6. OB4 and OB5 are very similar looking with comparable brightnesses. However, we caution that the uncertainty in measuring the outburst peak flux is high because of the method used to normalize these data. The shapes of the NOs are typical of those seen in other DNe (e.g. V344 Lyr; Cannizzo et al. 2010) consisting of a fast rise to peak brightness of between 0.81 and 1.25 d with a somewhat slower fall to quiescence taking 1.86–2.57 d.

3.2 The superoutburst

The SO we detected, OB2, is shown in Fig. 5. It reached peak flux on BJD 245 5176.86 and returned to quiescence 10.42 d later. We note that the SO was immediately preceded by a NO, OB1, which did not return to quiescent brightness before the onset of the SO. OB3 then occurred only 4 d after the SO returned to the quiescent flux level.

3.3 Superhumps

Superhumps always occur during SOs (e.g. Vogt 1980; Warner 2003; Kato et al. 2011). In NIK 1, the superhumps start during the decline of the NO, OB1, at the stage when the SO is likely beginning and continue until the OB3 begins.

We performed a Fourier transform of the SO searching for periods ranging from the Nyquist period (58.84 min) to 12 h. The strongest frequency (F_A) found is at 13.03 ± 0.03 cycles d^{-1} (1.842 ± 0.004 h) where the uncertainty was calculated using a Monte Carlo technique (Lenz & Breger 2005). In addition, we detect a signal at a frequency of 22.85 ± 0.08 cycles d^{-1} (= 1.05 h, F_B). The first overtone of the strongest frequency should occur at 26.06 cycles d^{-1} (F_2). However, because the Nyquist frequency (F_N) of the data is 24.47 cycles d^{-1}, we cannot uniquely detect F_2. The value of $F_2 - F_N$ is 1.59 ± 0.06 and $F_N - F_B$ is 1.62 ± 0.08; therefore, we concluded that the frequency at 22.85 cycles d^{-1} is very likely to be a reflection of the first overtone about the Nyquist frequency.

In order to better characterize the superhumps, we propagated the time series through a boxcar high-pass filter with a cut-off frequency of 18.0 d^{-1}. This is shown in the top panel of Fig. 7. We calculated a discreet short time Fourier transform (Harris 1978) over the duration of the SO. We used the filtered data and calculated a Fourier transform every 0.1 d with a siding window size of 2.0 d. The resulting power spectrum is shown in the lower panel of Fig. 7. Both F_A and F_B are visible for the entire duration of the SO and persist through the interval between OB2 and OB3. The superhump falls below a 3σ detection level at BJD 245 5190, close to the time OB3 begins. We do not detect the two signals over the rest of the time series with any significance.

In the upper two panels of Fig. 8 we zoom in around the two strongest frequencies seen in Fig. 7. The peak frequency of both the fundamental and reflection of the first overtone frequency vary over time. The crosses show the position of the maximum power in the sliding window power spectrum. In Q3, the period of the main peak and the reflection of the frequency of the first overtone appear to move in opposite directions. This is expected if the higher frequency peak is indeed a reflection about the Nyquist frequency. In the lower panel of Fig. 8 we show how the amplitude of both the fundamental (red crosses) and the reflection of the first overtone (blue crosses) change over time. The second harmonic frequency decays slower than the fundamental. The fundamental frequency falls below the 3σ detection level 0.6 d before the first overtone frequency.

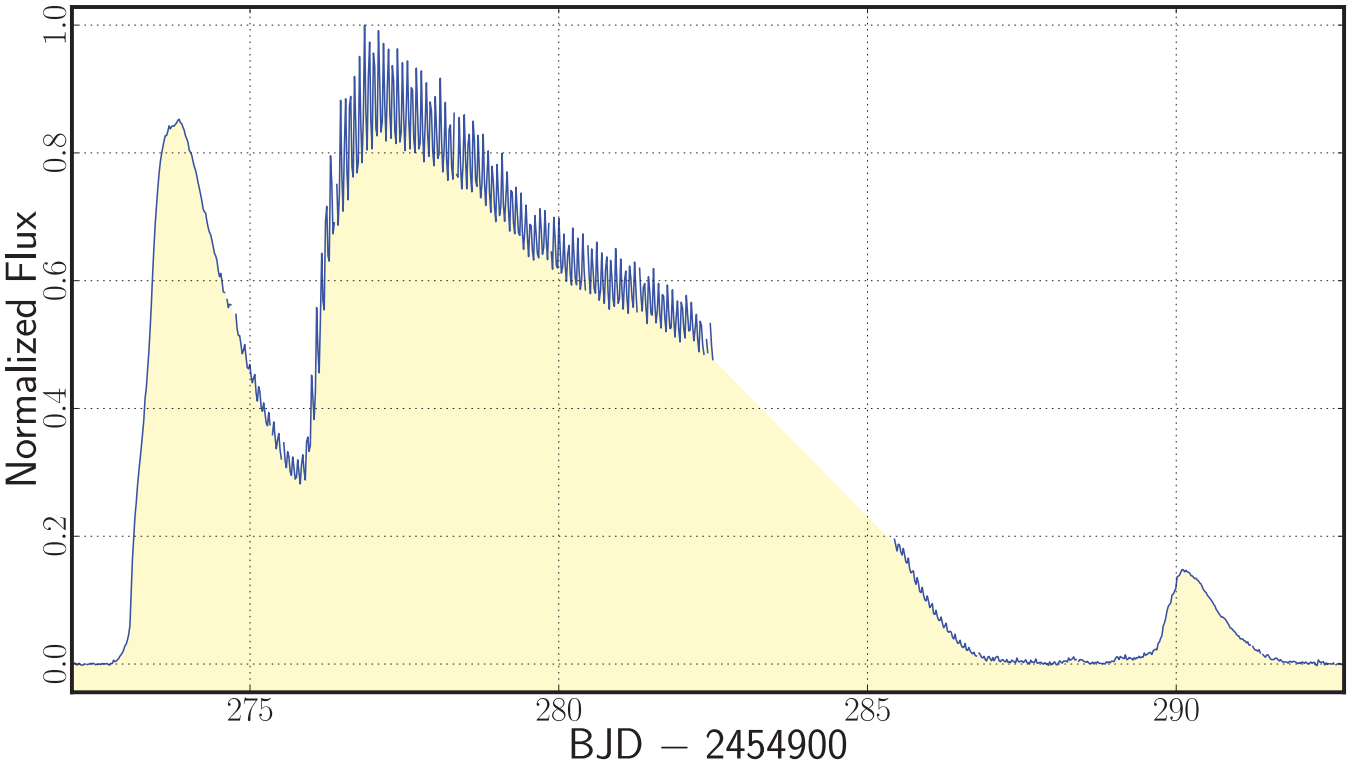

Figure 5. The corrected and normalized flux time series of NIK 1, in the region around OB1, OB2 and OB3. The SO is preceded by a NO, and 3 d after the SO we see a weaker NO. There is a gap in the data covering the SO from BJD 245 5182.5 to 245 5185.4 due to the quarterly roll of the spacecraft and data down link.

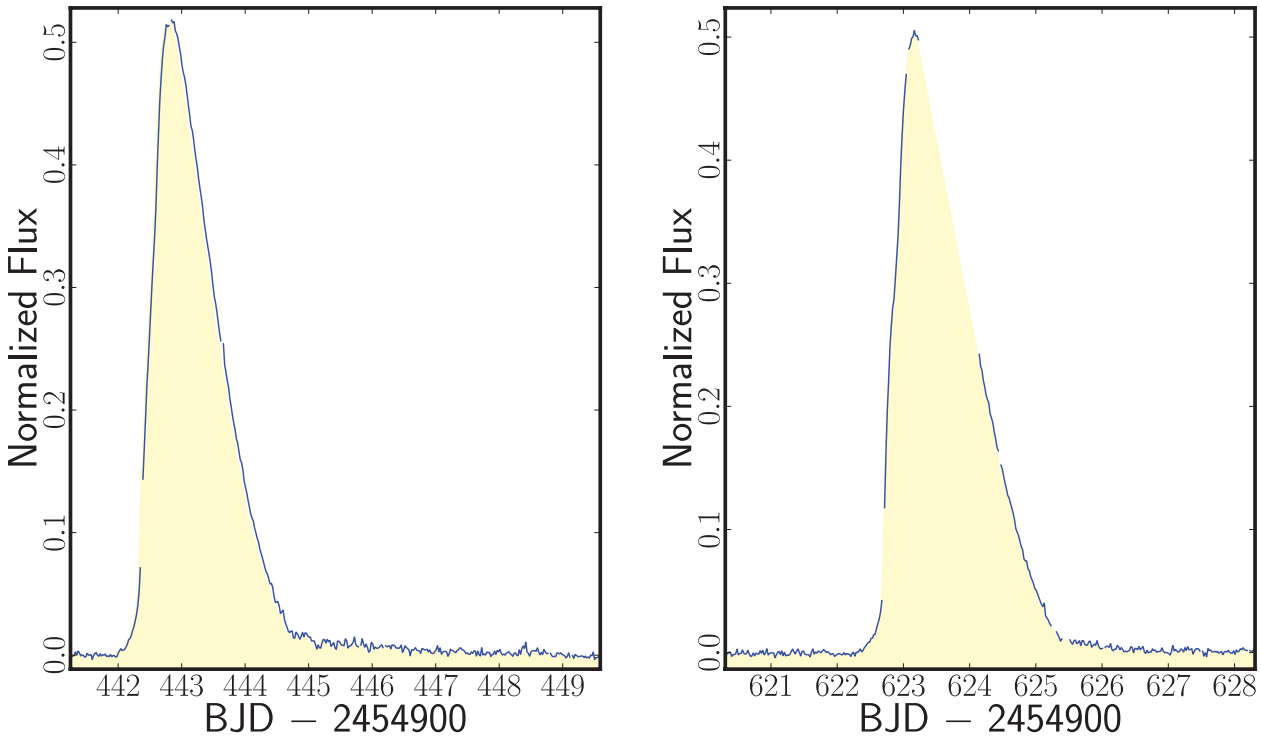

Figure 6. The corrected and normalized flux time series of NIK 1, zoomed in on the region around OB4 in the left-hand plot and OB5 in the right-hand plot. The large data gap in the OB5 plot is owing to the monthly Earth-point occurrence. No data are recorded during this time.

© 2012 The Authors, MNRAS **422,** 1219–1230
Monthly Notices of the Royal Astronomical Society © 2012 RAS

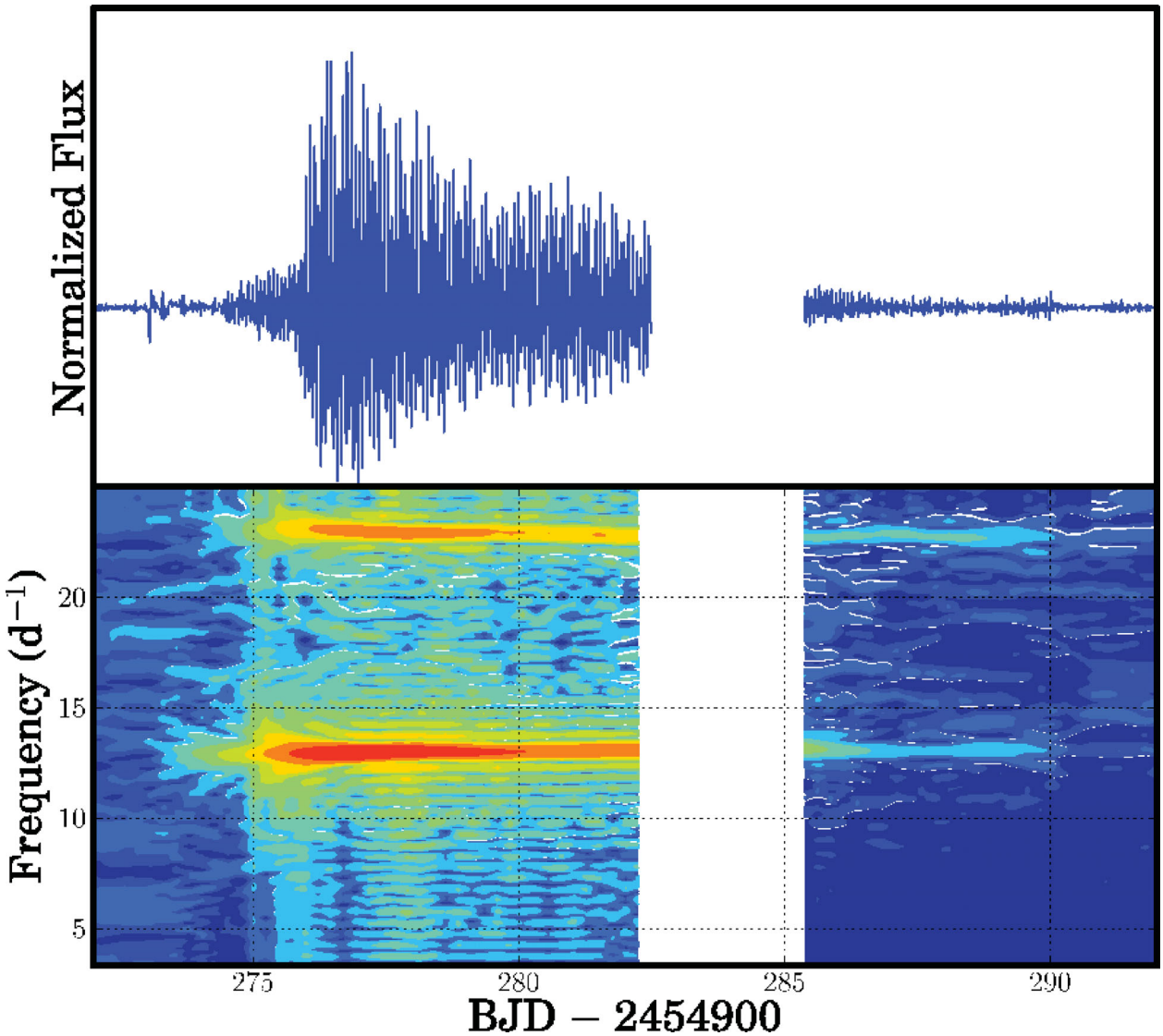

Figure 7. The upper panel shows the SO after being propagated through a high-pass filter. The lower panel shows a short time Fourier transform of the filtered data shown in the upper panel. Two periodic signals are detected: one at 1.842 h and the other at 1.05 h. These signals persist into the Q4 data and can be seen after the NIK 1 has faded before OB3 occurs.

We see changes in the superhump waveform when comparing the modulation at mid-outburst (top panel in Fig. 9), at the tail end of the SO (middle panel), and when the system is in a fainter state before the rise of OB3 (lower panel). The third time series is double peaked, which explains the reflection of the second harmonic decaying slower than the fundamental frequency in Fig. 8 – the waveform now has twice the frequency of the initial waveform.

4 DISCUSSIONS

4.1 The nature of the outbursts

NIK 1 is now the fourth CV which has been seen in outburst by *Kepler* (Still et al. 2010; Garnavich, Still & Barclay 2011; Kato et al. 2011). All four have undergone a SO. In two of the three other cases the SO has been immediately preceded by a NO (Still et al. 2010; Kato et al. 2011). In the third case, the rise of the SO is missed during a telescope safe mode (Garnavich et al. 2011). While statistics are still low this raises a question: are all SOs triggered by a NO?

Bateson (1977) suggested that in the DN VW Hyi, some SOs are triggered by a NO, and Marino & Walker (1979) posited that this is the case for all SOs of VW Hyi. In a few other ground-based observations of DN, the SO has been observed to be preceded by a NO – e.g. T Leo (Kato 1997), TV Crv (Uemura et al. 2005) and GO Com (Imada et al. 2004). Cannizzo et al. (2010) postulate that a NO occurs due to thermal instability in the disc, and, when there is enough mass built up from previous outbursts at large radial distances, a SO can be triggered. However, it takes time to propagate the heating front to large radii where this overdensity of material in the outer disc exists. We first see the NO and then when outer material transitions to the hot state, the SO occurs.

The limit cycle disc instability model predicts that the disc is much smaller directly after a SO and easier to excite into an outburst state. The intensity of outbursts should be lower and outbursts should occur more frequently for a smaller disc (Lasota 2001). Our observations are consistent with this pattern. We observe no

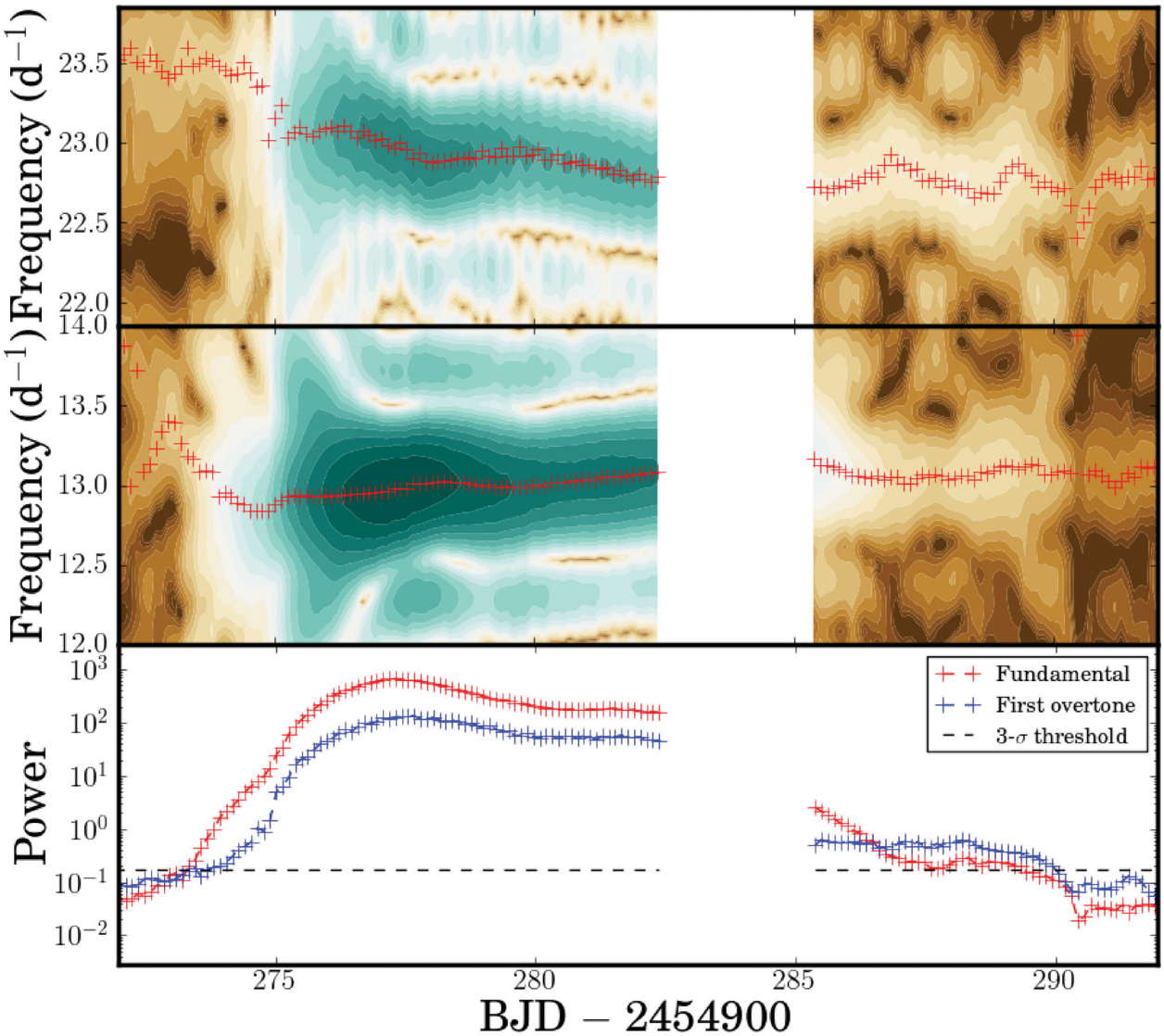

Figure 8. The discreet short time Fourier transform showing the two peaks identified in Fig. 7 in greater detail in the upper two panels. The red crosses show the position of the peak in the power spectrum in the region shown. The two panels' colours are scaled the same. The lower panel plots the peak power for both the fundamental frequency (red) and first overtone (blue). The black line is the 3σ detection threshold.

outbursts before OB1 – the system was quiescent for 208 d – and in the remaining observations the longest gap between outbursts is 181 d, the gap between OB4 and OB5, the final two outbursts. The NOs are more frequent after the SO and the spacing increases over time. We also see a much smaller outburst directly after the SO, which is consistent with theory.

We observed superhumps lasting for ∼17 d. They begin during the fading of the NO which preceded the SO and last until the beginning of OB3. We see superhumps for 3–4 d after the SO has faded to quiescence. There have only been four other reports of superhump persisting after the end of a SO: V1159 Ori (Patterson et al. 1995), ER UMa (Gao et al. 1999), EG Cnc (Patterson et al. 1998) and V344 Lyr (Still et al. 2010). It seems likely material will persist at large radii well after the majority of material has been accreted by the white dwarf, and the reason superhumps have been seen persisting so few times is because of a lack of sensitivity in ground-based observations.

The disc instability model (Osaki 1989; Lasota 2001) predicts two main sources driving the superhump modulation: viscous dissipation within a flexing disc driven by the compression of the disc opposite the secondary star, and the hotspot where the accretion stream impacts the disc sweeping around the rim of a non-axisymmetric disc (Wood et al. 2011). During the *early superhumps*, the hotspot signal is much weaker than the signal from the disc and the phase curve is single peaked. As the disc fades, the hotspot from the impact of the accretion stream on to the disc will become brighter relative to the disc because the disc has been drained of material and so is much less luminous.

We see the sumperhump waveform change over the course of the SO. In the folded time series shown in the upper panel of Fig. 9, the waveform is asymmetric, and the pulse rises around twice as fast as it falls. The shape is very similar to that seen in V344 Lyr (Still et al. 2010) at a comparable time in the SO evolution and in the simulations shown in fig. 1 of Wood et al. (2011) when modelling

© 2012 The Authors, MNRAS **422,** 1219–1230
Monthly Notices of the Royal Astronomical Society © 2012 RAS

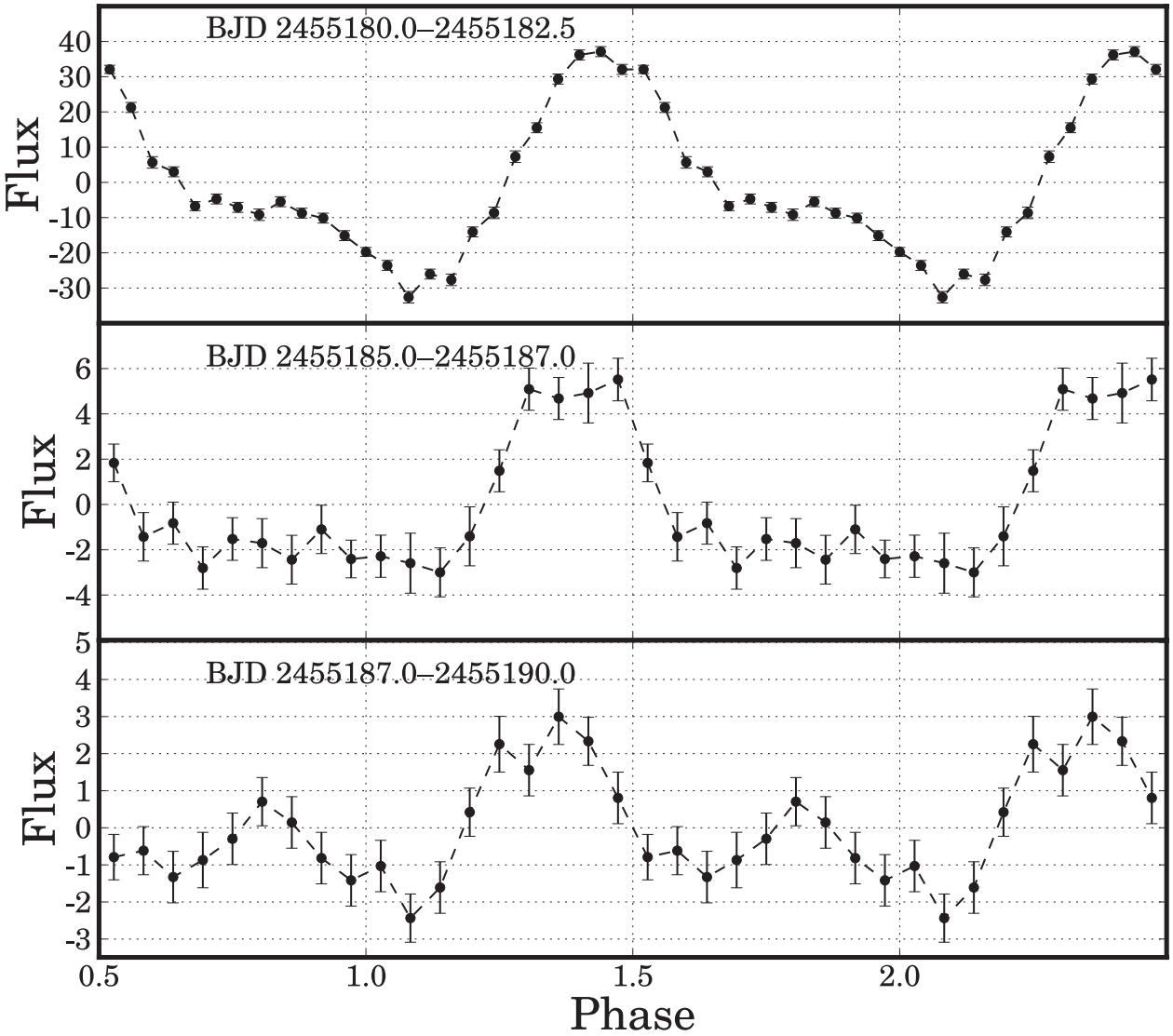

Figure 9. Three sections of the light curve of NIK 1 folded on a period of 1.842 h and binned. The top panel covers the end of the last 2.5 d of the Q3 data, the middle panel the tail of the SO, which is the first 2 d of Q4 and the lower panel covers the quiescent period after the SO and rise of OB3. The flux levels are arbitrary but are internally consistent between the three plots.

early superhumps. In the middle panel, we see some evolution of the waveform and we no longer see evidence for the asymmetry; the light curve is similar to that seen in fig. 3 of Wood et al. (2011) where they have accretion stream impact in the model. Our assumption is that in the middle panel we are seeing no variable component from the accretion stream.

The waveform changes in the lower panel of Fig. 9. Similarly to the other panels there is a peak around phase 0.9 – any difference can be attributed to the error on the period on which the data were folded. However, there is also a secondary peak which is offset in phase by ∼180° and of lower intensity than the main peak. This is wholly consistent with fig. 2 of Wood et al. (2011) where both the disc and the hotspot contribute to the emission for the system.

Given that orbital periods are typically a few per cent lower than the superhump period (Warner 2003), we can place an upper limit on the binary orbital period of 1.842 ± 0.004 h; this places NIK 1 below the period gap. This meets expectations as almost all SU UMa stars are below the period gap (Kato et al. 2011).

4.2 DNe in the *Kepler* field of view

What is the possibility of finding more DNe as background sources in the *Kepler* data? Using the empirical relation of Patterson (2011), the lowest peak absolute magnitude of a DN outburst in a system with a period longer than 90 min is $M_V = 5.3$. This implies *Kepler* can observe DNe in outburst out to a distance of 8.7 kpc if we assume we can observe all sources with a peak brightness $Kp < 20$, which is approximately the source confusion limit of *Kepler*. However, we cannot assume an isotropic distribution out to this distance. Instead, we restrict our search to only sources less than 300 pc above the Galactic plane, which Patterson (2011) estimates to be the scale height for DNe.

The centre of the *Kepler* field of view is 13°.5 above the Galactic plane and the field of view is 116 deg^2 (Koch et al. 2010). Therefore, the greatest distance an observable DN can be from Earth and still be within our scale height constraint is 1285 pc, and our search volume is 2.5×10^7 pc^3 (this includes the entire field of view,

Table 4. The number of DNe predicted to be within one scale height of the Galaxy and in the *Kepler* field of view are given in this table. We use two estimates of the scale height: 300 and 150 pc. Likewise, we use six different estimates of the space density which range from 1.8×10^{-6} to 10^{-4} pc^{-3}.

Space density (DN pc^{-3})	Sources in focal plane scale height (pc) 300 (1)	150 (2)	Sources in downloaded data scale height (pc) 300 (1)	150 (2)
1.8×10^{-6} (1)	44.9	5.6	2.6	0.32
7.9×10^{-6} (2)	196.8	24.6	11.3	1.4
1.1×10^{-5} (3)	274.1	34.3	15.8	2.0
2.1×10^{-5} (4)	523.4	65.4	30.1	3.8
10^{-4}(5)	2492	311.5	143.3	17.9
1.8×10^{-4} (3,6)	4485	560.7	257.9	32.2

References. (1) Patterson (2011); (2) Ak et al. (2008); (3) Pretorius et al. (2007); (4) Hertz et al. (1990); (5) Shara et al. (1993); (6) Kolb (1993).

not just the pixels downloaded). The period luminosity relation of Patterson (2011) predicts all DNe outbursts in our search volume will be brighter than $V = 15.8$ and easily be detected by *Kepler*, even if they have high reddening.

Patterson (2011) gives a lower limits to the space density at DNe of 1.8×10^{-6} pc^{-3} , but this value is calculated using only 42 systems with known distance and most likely underpredicts the true value significantly. Other estimates from observations include 7.9×10^{-6} pc^{-3} (Ak et al. 2008), 1.1×10^{-5} pc^{-3} (Pretorius et al. 2007), 2.1×10^{-5} pc^{-3} (Hertz et al. 1990) and 10^{-4} pc^{-3} (Shara et al. 1993). Theoretically, the number is thought to be around 1.8×10^{-4} pc^{-3} (Kolb 1993; Pretorius et al. 2007). For each of these estimates we have calculated the inferred number of DNe potentially visible to *Kepler*. These are given in Table 4 and assume an isotropic distribution within the search range of one Galactic disc scale height.

Ak et al. (2008) measure the scale height of the DN population to be only 150 ± 18 pc. If we use this value as the ceiling of our search, the numbers predicted decrease by a factor of 8. These values are also shown in Table 4.

The predicted values range from 6 to 4485, which leads us to believe that the true space density of DNe is wholly unconstrained.

If we are considering systems that may be found as background sources in apertures of target stars, the numbers decrease by a factor of $\sim$17 because *Kepler* only downloads the pixels from 5.75 per cent of the focal plane. With this restriction, the predicted number in *Kepler* ranges from 0.3 to 258. With only nine known DNe in the data, we are unable to rule out any of the models at the 3σ level. The predictions are likely to be an underestimate of the true number because this estimate would not include the source in this work as it would be further than 300 pc from the Galactic equator. A systematic search of the target pixel files may lead to a bounty of new DNe. Such work will help constrain the true value of the space density of DNe.

5 SUMMARY

We have serendipitously observed outbursts of a DN which was captured within the aperture of a G-type star. We first extracted the flux of this source from the target pixel files and then removed systematic trends from the data using CBVs. We observed four NO and one SO over 22 months. The SO was likely triggered by a NO. We observed superhumps during the SO and saw the waveform change from being single peaked to double peaked over the course of the outburst, which we attribute to the appearance of the accretion stream impact on to the disc.

Given that this DN was observed as a background source, we used various predictions of DNe space density to predict the number of DNe in the *Kepler* field of view and in data already collected. The models vary wildly from predicting 4485 and 257.9 in the field of view and in collected data, respectively, to 2.6 and 0.32. A detailed study of the background pixels collected by *Kepler* could be used to constrain the space density of DNe.

ACKNOWLEDGMENTS

Kepler was selected as the 10th Discovery mission. Funding for *Kepler* is provided by NASA's Science Mission Directorate. This paper made extensive use of the PyKE tools provided by the Kepler Guest Observer Office for the use of the community. All of the data presented in this paper were obtained from the Multimission Archive at the Space Telescope Science Institute (MAST). STScI is operated by the Association of Universities for Research in Astronomy, Inc., under NASA contract NAS5-26555. Support for MAST for non-*HST* data is provided by the NASA Office of Space Science via grant NNX09AF08G and by other grants and contracts. We used images from The Digitized Sky Surveys which were produced at the Space Telescope Science Institute under US Government grant NAG W-2166. The images of these surveys are based on photographic data obtained using the Oschin Schmidt Telescope on Palomar Mountain and the UK Schmidt Telescope. The plates were processed into the present compressed digital form with the permission of these institutions.

REFERENCES

Ak T., Bilir S., Ak S., Eker Z., 2008, New Astron., 13, 133
Balbus S. A., Hawley J. F., 1998, Rev. Modern Phys., 70, 1
Barclay T. et al., 2011, Kepler Data Release 12 Notes, KSCI-19052-001
Bateson F. M., 1977, New Zealand J. Sci., 20, 73
Borucki W. J. et al., 2010, Sci, 327, 977
Brown T. M., Latham D. W., Everett M. E., Esquerdo G. A., 2011, AJ, 142, 112
Cannizzo J. K., 1993, ApJ, 419, 318
Cannizzo J. K., Still M. D., Howell S. B., Wood M. A., Smale A. P., 2010, ApJ, 725, 1393
Christiansen J. L. et al., 2011a, Kepler Data Characteristics Handbook, KSCI-19040-002
Christiansen J. L. et al., 2011b, Kepler Data Release 11 Notes, KSCI-19051-001
Downes R. A., Webbink R. F., Shara M. M., Ritter H., Kolb U., Duerbeck H. W., 2001, PASP, 113, 764
Fraquelli D., Thompson S. E., 2011, Kepler Archive Manual, KDMC-10008-003
Gao W., Li Z., Wu X., Zhang Z., Li Y., 1999, ApJ, 527, L55
Garnavich P., Still M., Barclay T., 2011, Astron. Telegram, 3507, 1
Gilliland R. L. et al., 2011, ApJS, 197, 6
Harris F., 1978, Proc. IEEE, 66, 51
Hellier C., 2001, in Hellier C., ed., Cataclysmic Variable Stars. Springer-Praxis, Chichester
Hertz P., Bailyn C. D., Grindlay J. E., Garcia M. R., Cohn H., Lugger P. M., 1990, ApJ, 364, 251
Hōshi R., 1979, Progress Theor. Phys., 61, 1307
Imada A. et al., 2005, PASJ, 57, 193
Kato T., 1997, PASJ, 49, 583
Kato T. et al., 2011, preprint (arXiv:1108.5252)
Koch D. G. et al., 2010, ApJ, 713, L79
Kolb U., 1993, A&A, 271, 149
Lasota J.-P., 2001, New Astron. Rev., 45, 449

Lenz P., Breger M., 2005, Commun. Asteroseismol., 146, 53
Marino B. F., Walker W. S. G., 1979, in Bateson F. M., Smak J., Urch I. H., eds, IAU Colloquial 46, Changing Trends in Variable Star Research. Univ. Waikato, Hamilton, p. 29
Monet D. G. et al., 2003, AJ, 125, 984
Osaki Y., 1989, PASJ, 41, 1005
Patterson J., 2011, MNRAS, 411, 2695
Patterson J., Jablonski F., Koen C., O'Donoghue D., Skillman D. R., 1995, PASP, 107, 1183
Patterson J. et al., 1998, PASP, 110, 1290
Pretorius M. L., Knigge C., O'Donoghue D., Henry J. P., Gioia I. M., Mullis C. R., 2007, MNRAS, 382, 1279
Quintana E. V. et al., 2010, Proc. SPIE, 7740, 77401X
Ramsay G. et al., 2009, MNRAS, 398, 1333
Ritter H., Kolb U., 2003, A&A, 404, 301
Sekiguchi K., 1992, Nat, 358, 563
Shakura N. I., Sunyaev R. A., 1973, A&A, 24, 337
Shara M., Moffat A., Potter M., Bode M., Stephenson F. R., 1993, in Regev O., Shaviv G., eds, Ann. Israel Phys. Soc., 10, 84
Smak J., 1984, Acta Astron., 34, 161
Still M., Howell S. B., Wood M. A., Cannizzo J. K., Smale A. P., 2010, ApJ, 717, L113
Thorstensen J. R., Lépine S., Shara M., 2006, PASP, 118, 1238
Twicken J. D., Chandrasekaran H., Jenkins J. M., Gunter J. P., Girouard F., Klaus T. C., 2010, Proc. SPIE, 7740, 77401U
Uemura M. et al., 2005, A&A, 432, 261
Vogt N., 1980, A&A, 88, 66
Warner B., 2003, Warner B., ed., Cataclysmic Variable Stars. Cambridge Univ. Press, Cambridge
Whitehurst R., 1988, MNRAS, 232, 35
Wood M. A., Still M. D., Howell S. B., Cannizzo J. K., Smale A. P., 2011, ApJ, 741, 105

This paper has been typeset from a TEX/LATEX file prepared by the author.